Available online at www.sciencedirect.com
ScienceDirect
Journal of Power Sources 179 (2008) 200–208
JOURNAL OF POWER SOURCES
www.elsevier.com/locate/jpowsour

Analytic determination of the effective thermal conductivity of PEM fuel cell gas diffusion layers

E. Sadeghi *, M. Bahrami, N. Djilali

Department of Mechanical Engineering and the Institute for Integrated Energy Systems, University of Victoria, Victoria, BC V8W 3P6, Canada

Received 10 October 2007; received in revised form 14 December 2007; accepted 18 December 2007
Available online 26 December 2007

Abstract

Accurate information on the temperature field and associated heat transfer rates are particularly important in devising appropriate heat and water management strategies in proton exchange membrane (PEM) fuel cells. An important parameter in fuel cell performance analysis is the effective thermal conductivity of the gas diffusion layer (GDL). Estimation of the effective thermal conductivity is complicated because of the random nature of the GDL micro structure. In the present study, a compact analytical model for evaluating the effective thermal conductivity of fibrous GDLs is developed. The model accounts for conduction in both the solid fibrous matrix and in the gas phase; the spreading resistance associated with the contact area between overlapping fibers; gas rarefaction effects in microgaps; and salient geometric and mechanical features including fiber orientation and compressive forces due to cell/stack clamping. The model predictions are in good agreement with existing experimental data over a wide range of porosities. Parametric studies are performed using the proposed model to investigate the effect of bipolar plate pressure, aspect ratio, fiber diameter, fiber angle, and operating temperature.
© 2007 Elsevier B.V. All rights reserved.

Keywords: Porous media; Gas diffusion layer; PEM fuel cell; Spreading resistance; Effective thermal conductivity

1. Introduction

Electrochemical energy conversion in hydrogen fuel cells is an exothermic process that results in significant temperature variations [1,2]. Accurate information on the temperature field and associated heat transfer rates are particularly important in devising appropriate heat and water management strategies in proton exchange membrane (PEM) fuel cells, as the temperature field affects relative humidity, membrane water content, and reaction kinetics, as well as durability. One of the main fuel cell components in this respect is the porous gas transport layer, commonly referred to the gas diffusion layer (GDL). GDLs employed in PEM fuel cells typically consist of a fibrous structure in the form of a thin "paper" or "woven cloth", see Fig. 1. The GDL provides five key functions for a PEM fuel cell: (1) mechanical support, (2) electronic conductivity, (3) heat removal, (4) reactant access to catalyst layers, and (5) product removal [3].

The porous nature of GDL micro structure, makes it necessary to define an effective thermal conductivity, a transport parameter that plays an important role in fuel cell performance analysis [4] and that is required in computational models [5]. In addition to being porous, GDLs are anisotropic, which adds to the complexity of characterizing the effective thermal conductivity.

Ramousse et al. [4] recently investigated the effective thermal conductivity of non-woven carbon felt GDLs and estimated the conductivity bounds using a model connecting the two phases (solid and gas) in series or parallel. The model as well as their experimental measurements yielded conductivity values that are at least one order of magnitude lower than most values reported in the literature. Ramousse et al. [4] also noted that due to contact and constriction resistances between carbon fibers, the effective thermal conductivity of carbon felts are much lower than pure

* Correspondingauthor. Tel.: +1 250 813 3125; fax: +1 250 721 6051.
E-mail addresses: ehsans@uvic.ca (E. Sadeghi), mbahrami@uvic.ca (M. Bahrami), ndjilali@uvic.ca (N. Djilali).

0378-7753/$ – see front matter © 2007 Elsevier B.V. All rights reserved.
doi:10.1016/j.jpowsour.2007.12.058

Nomenclature

A	area (m^2)
a, b	major and minor semi axes of elliptical contact area (m)
d	fiber diameter (m)
E	Young's modulus (Pa)
E'	effective elastic modulus (Pa)
F	contact load (N)
F_1	integral function of $(\rho'\rho''^{-1})$, Eq. (8)
GDL	gas diffusion layer
$K(\cdot)$	complete elliptic integral of the first kind
k	thermal conductivity ($Wm^{-1}\,K^{-1}$)
k_{eff}	effective thermal conductivity ($Wm^{-1}\,K^{-1}$)
k_{eff_0}	effective thermal conductivity of the reference basic cell ($Wm^{-1}\,K^{-1}$)
k^*	non-dimensional effective thermal conductivity, $k_{eff}\,k_{eff_0}^{-1}$
l	distance between two adjacent fibers in x-direction (Fig. 3) (m)
P_{BP}	bipolar pressure (Pa)
P_g	gas pressure (Pa)
P_{GDL}	GDL pressure (Pa)
Pr	Prandtl number (–)
Q_{gc}	heat transfer rate through gas filled gap (W)
R	thermal resistance (KW^{-1})
R_{co}	constriction resistance (KW^{-1})
R_{sp}	spreading resistance (KW^{-1})
T	temperature (K)
V_s	fiber (solid) volume of basic cell (m^3)
V_{tot}	total volume of basic cell (m^3)
w	distance between two adjacent fibers in the y-direction (Fig. 3) (m)

Greek

α	thermal accommodation parameter
β	fluid property parameter, Eq. (17)
$\delta(x)$	local gap thickness (m)
ε	porosity (–)
η	modulus of elliptic integral (–)
γ	heat capacity ratio (–)
Λ	mean free path of gas molecules (m)
λ	ratio of relative radii of curvature $(\rho'\rho''^{-1})$
μ	ratio of molecular weights of the gas and the solid, $M_g\,M_s^{-1}$
θ	angle between two fibers (rad)
ρ', ρ''	major and minor relative radii of curvature (m)
ρ'_1, ρ'_2	principal radii of curvature (m)
ρ_e	equivalent radius of curvature of the contacting surfaces (m)
υ	Poisson's ratio (–)
ξ	aspect ratio (wl^{-1})

Subscripts

0	reference state
1	bottom block of the basic cell
2	top block of the basic cell
∞	standard condition state
c	contact plane
g	gas
gc	gas filled gap
max	maximum value
s	solid (carbon fiber)
t	upper boundary of the top block
tot	total value

carbon, and used Danes and Bardon [6] correlation to estimate the effective thermal conductivity of the solid phase.

Khandelwal and Mench [7] measured the through-plane thermal conductivity of GDLs. They examined two different types of commercial GDLs with a variety of thickness and porosity. They studied the effect of temperature and polytetrafluoro ethylene (PTFE) content on the effective thermal conductivity, and obtained values in close agreement with the manufacturer data sheet. The experimental data reported in the literature for effective thermal conductivity spans a wide range of values, 0.1–1.6 $Wm^{-1}\,K^{-1}$, and there is clearly need to better understand of the possible sources of inconsistency [1,4].

Our literature review indicates the need for a general model that can accurately predict the effective thermal conductivity of GDL, and its trends as parameters varied, since no reliable correlations are available and there is lack of data and understanding on the effect of geometric parameters such as tortuosity, radius of contact area between fibers, and angle between fibers. The objectives of the present work are:

- Develop and verify a comprehensive analytical model that can predict the effective thermal conductivity of GDLs and that captures accurately the trends observed in experimental data.
- Investigate the effect of relevant geometrical, thermal, and mechanical parameters involved and identify the controlling parameters.

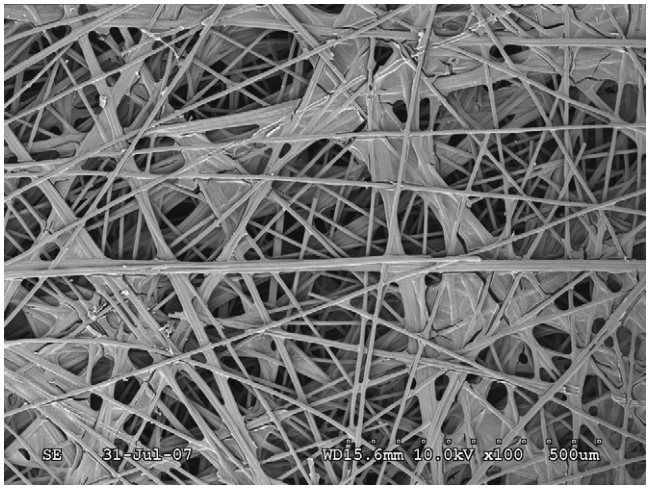

Fig. 1. SEM image of a Toray GDL.

Following the approach used successfully in several applications such as spherical packed beds by Bahrami et al. [8], a "basic cell" is taken to represent the fibrous media, i.e. the structure is assumed to be repeated throughout the GDL. Each cell is made up of contact regions. A contact region is composed of a contact area between two portions of fibers, surrounded by a gas (air) layer. A thermal resistance model is then constructed taking into account the basic conduction processes through both the solid fibrous matrix and the gas phase as well as important phenomena including spreading resistance associated with the contact area between overlapping fibers and gas rarefaction effects in microgaps.

The basic cell approach breaks the problem into distinct conduction paths, the contact between two fibers, the gas layer between fibers; and calculates the conductivity of the medium as a series/parallel combination of the individual resistances for those paths. The advantage of this approach is that it readily allows evaluation of the relative contributions of each conduction path as a function of the medium properties [8].

The scheme of the present approach to evaluate the effective thermal conductivity is shown in Fig. 2. The first step in estimating the effective thermal conductivity is the reconstruction of the GDL geometrical structure. The GDL is represented as cylindrical carbon fibers that are equally spaced horizontally and stacked vertically to form mechanical contacts, Fig. 3. The next step is mechanical modeling of the contacting fibers. The Hertzian theory [9] is used to evaluate the contact area between fibers, and a thermal resistance network is constructed to account for the effective thermal conductivity, allowing analytic determination of the effective thermal conductivity. The results of the model are compared to experimental data. Moreover, parametric study is then performed to investigate the effect of key parameters on the effective thermal conductivity of GDLs.

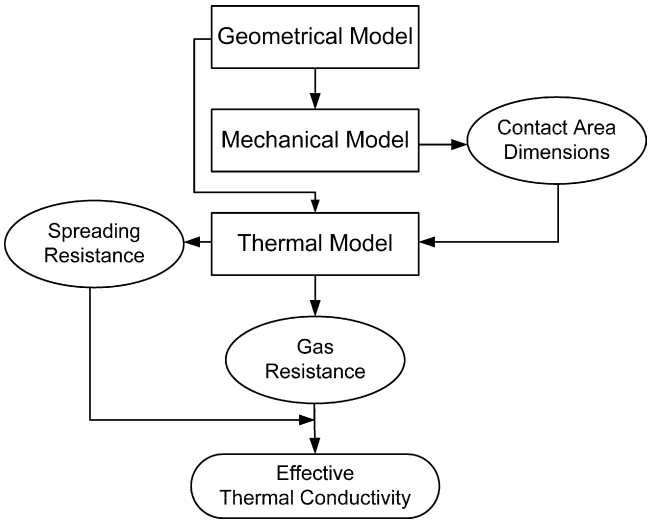

Fig. 2. Model development.

2. Model development

Both electrical and thermal conductivity of carbon paper GDLs are orthotropic [4,10], with in-plane conductivity that are an order of magnitude higher than the through plane value. The thermal field and heat transfer rates depend on a variety of factors including, geometry, material properties of the various components and operating conditions, the heat transfer in the GDL is however generally limited by the through plane conductivity value on which we focus our analysis. The model considers the GDL to consist of a periodic fibrous micro structure and assumes:

(1) 3-D repeating basic cell, Fig. 3.
(2) Steady state one-dimensional heat transfer.
(3) Negligible natural convection; justified by the Grashof number for a typical GDL with fiber diameter of 8.5 μm which is in order of 10^{-6} and is significantly lower than 2500, the limit for natural convection [11].
(4) No radiation heat transfer. PEM fuel cells typically operate between 60 and 90 °C, and the contribution of radiation is small and can be neglected.

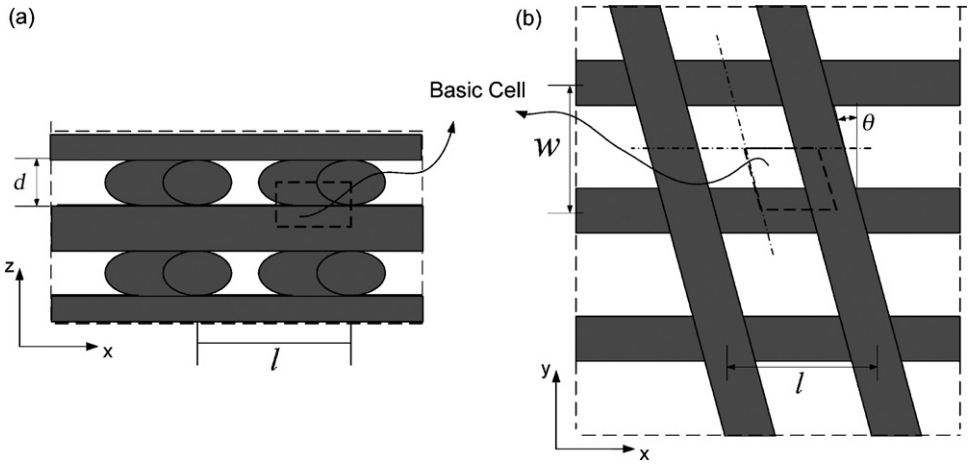

Fig. 3. (a) Front view and (b) top view of the geometrical model of GDL.

(5) Regular fiber surfaces (no roughness or out-of-flatness for contacting fibers).

Based on these assumptions, we propose a resistance network model for conduction through the solid and gas phases which accounts for geometric structure, effect of compression, gas rarefaction effect (in microgaps between fibers), and spreading resistance.

2.1. Geometrical model

Fig. 1 shows SEM image of a Toray GDL that clearly illustrates the random and anisotropic structure. The proposed geometrical model is an idealization shown in Fig. 3 and consists of uniformly sized equally spaced cylindrical fibers immersed in stagnant air. The fibers angle, θ, is variable in this model.

The porosity is defined as:

$$\varepsilon = 1 - \frac{V_s}{V_{tot}} \tag{1}$$

where V_s and V_{tot} are the volume of fibers and the basic cell, respectively. Calculating these volumes based on the basic cell geometry in Fig. 3 yields:

$$\varepsilon = 1 - \frac{\pi d}{8}\left[\frac{l + (w/\cos\theta)}{lw}\right] \tag{2}$$

2.2. Mechanical model

Thermal energy transfers from one fiber to another through the contact interface, and resistance to heat conduction depends on the contact area dimensions. In order to determine the contact area dimensions, the Hertzian theory [9] is used in the present study.

The general shape of the contact area is elliptical; when $\theta = 0$, the contact area becomes circular. Applying the Hertzian theory [9], the semi-axes of the contact area are given by:

$$b = \left(\frac{\rho''}{\rho'}\frac{3F\rho_e}{4E'}\right)^{1/3} F_1 \tag{3}$$

$$a = b\left(\frac{\rho'}{\rho''}\right)^{2/3} \tag{4}$$

where a and b are the major and minor semi-axes of the elliptical contact area, respectively; ρ_e is the equivalent radius of curvature, $\rho_e = \sqrt{\rho'\rho''}$ [9]; and E' is a modulus incorporating the fibers Young's modulus and Poisson's ratio.

$$E' = \left(\frac{1-\nu_1^2}{E_1} + \frac{1-\nu_2^2}{E_2}\right)^{-1} \tag{5}$$

ρ' and ρ'' are the major and minor relative radii of curvature at the contact point expressed as [9]:

$$\rho'' = \frac{d}{\sqrt{2(1-\cos 2\theta)} + 2} \tag{6}$$

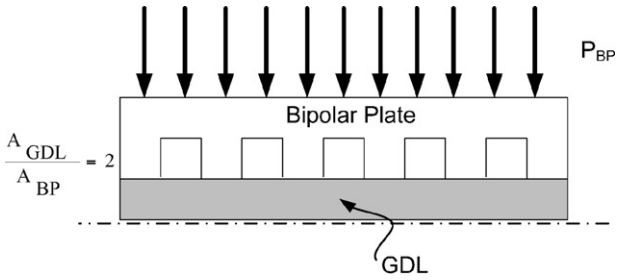

Fig. 4. Pressure distribution on the bipolar plate and GDL.

$$\rho' = \frac{1}{(4/d) - (1/\rho'')} \tag{7}$$

F_1, the parameter used in Eq. (3), is a complex integral function of ($\lambda = \rho'/\rho''$) [9]. We correlate this integral and propose the following relationship:

$$F_1 = \frac{19.1\sqrt{\lambda}}{1 + 16.76\sqrt{\lambda} + 1.34\lambda} \tag{8}$$

The accuracy of the relationship is within 0.08%.

In order to determine the contact area dimensions, the magnitude of the contact force is required. This force F can be evaluated from the clamping pressure applied via the fuel cell bipolar plates. The land/flow channel area ratio used in PEM fuel cells is optimized to balance electrical conduction and mass transport and is typically of order 1 as shown in Fig. 4. Thus the maximum pressure to which the GDL is subjected is twice that of the bipolar plate, i.e. $P_{GDL} = 2P_{BP}$. As shown in Fig. 3, a cell with the cross-sectional area of lw consists of four contact points; therefore, the corresponding maximum force on each contact is:

$$F_{max} = \frac{P_{GDL}\, lw}{4} \tag{9}$$

2.3. Thermal model

Based on the assumptions discussed in Section 2, a thermal resistance network corresponding to the basic cell is constructed as shown in Fig. 5 by considering the top and bottom blocks of the basic cell structure. The thermal resistances in the network represent the heat transfer paths through the gas and carbon fibers, see Fig. 6. The solid bulk resistance is small compared with the gap resistance and its effect on the total resistance is negligible and not accounted.

2.3.1. Thermal constriction/spreading resistance

Thermal constriction/spreading resistance is defined as the difference between the average temperature of the contact area and the average temperature of the heat source/sink, which is located far from the contact area, divided by the total heat flow rate Q [12].

$$R_{co} = R_{sp} = \frac{\Delta T}{Q} \tag{10}$$

If the contact areas are small compared with the distance separating them, the heat source on a half-space solution can

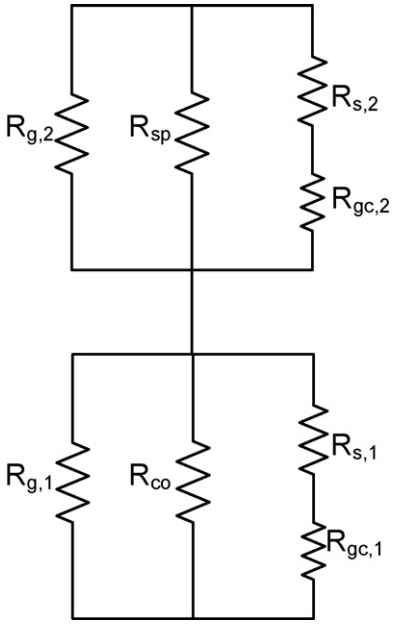

Fig. 5. Thermal resistance network for the top and bottom blocks of the basic cell.

be used [13]. Fig. 7 illustrates the geometry of a circular heat source on a half-space.

The spreading resistance for an isothermal elliptical contact area can be determined analytically [14]:

$$R_{sp} = \frac{1}{2\pi ka} K(\eta) \tag{11}$$

where $\eta = \sqrt{1-(b/a)^2}$ and $K(\eta)$ is the complete elliptic integral of the first kind of modulus η.

$$K(\eta) = \int_0^{\pi/2} \frac{\mathrm{d}t}{\sqrt{[1-\eta^2 \sin^2 t]}} \tag{12}$$

2.3.2. Gas resistance

Gas resistance can be decomposed into two parallel resistances for each block, see Fig. 6. Kennard [15] modeled the gas conduction between two parallel plates for temperature jump

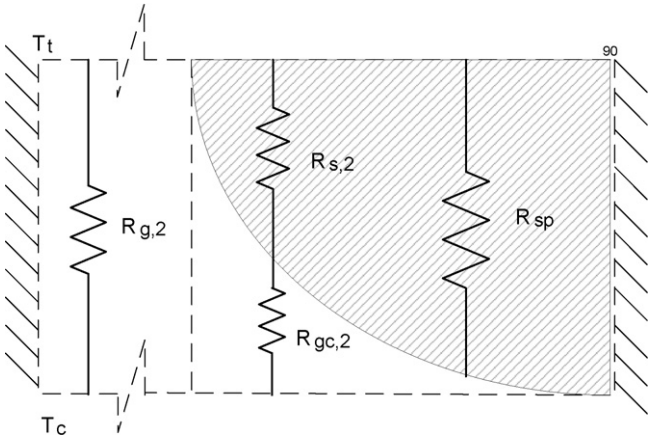

Fig. 6. Thermal resistances for the top block of the basic cell.

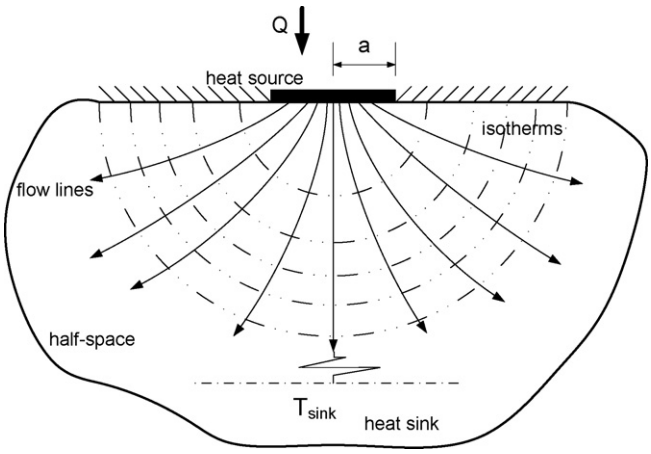

Fig. 7. Circular heat source on a half-space.

as $Q_{gc} = k_g A \Delta T/(\delta + M)$. Yovanovich [16] showed that this expression can be used for all possible regimes. We assume that heat conduction at each differential element, dx, is similar to that between parallel plates; therefore, using Kennard's expression for each differential element, we find:

$$\mathrm{d}Q_{gc} = k_g \left(\frac{w}{2}\right) \frac{\Delta T(x)}{\delta(x) + M} \mathrm{d}x \tag{13}$$

The gas parameter M is defined as:

$$M = \alpha\beta\Lambda \tag{14}$$

The mean free path Λ of the gas molecules can be expressed in terms of $\Lambda_{g,\infty}$, the mean free path of gas molecules at the reference state.

$$\Lambda = \Lambda_{g,\infty} \left(\frac{T_g}{T_{g,\infty}}\right) \left(\frac{P_{g,\infty}}{P_g}\right) \tag{15}$$

with $T_{g,\infty} = 25^\circ$ C and $P_{g,\infty} = 1$ atm. The thermal accommodation parameter α and the fluid property parameter β are defined by:

$$\alpha = \left(\frac{2-\alpha_1}{\alpha_1}\right) + \left(\frac{2-\alpha_2}{\alpha_2}\right) \tag{16}$$

$$\beta = \frac{2\gamma}{Pr(\gamma+1)} \tag{17}$$

where γ is the ratio of specific heats, Pr is the Prandtl number, and α_1, α_2 are thermal accommodation coefficients of the top and bottom surfaces. Here, the top surface corresponds to carbon fiber and the bottom to the gas, i.e. $\alpha_1 = \alpha_s$ and $\alpha_2 = 1$,

$$\alpha = \left(\frac{2-\alpha_s}{\alpha_s}\right) + 1 \tag{18}$$

Song and Yovanovich [17] experimentally correlated the thermal accommodation coefficient.

$$\alpha_s = \exp\left[-0.57\left(\frac{T_s - 273}{273}\right)\right] \left(\frac{1.4M_g}{6.8 + 1.4M_g}\right) + \frac{2.4\mu}{(1+\mu)^2} \times \left\{1 - \exp\left[-0.57\left(\frac{T_s - 273}{273}\right)\right]\right\} \tag{19}$$

where $\mu = M_g/M_s$; M_g and M_s are molecular weights of the gas and the solid.

The total heat flow through the gas-filled gap, gas filled between the quarter cylindrical fiber and the separating plane, is given by the integral

$$Q_{gc} = k_g \left(\frac{w}{2}\right) \int_0^{d/2\cos\theta} \frac{\Delta T(x)}{\delta(x) + M} dx \quad (20)$$

The thermal resistance of the gas-filled gap, $R_{gc,2}$, is defined in terms of the temperature difference between two bounding surfaces, ΔT_c.

$$\frac{1}{R_{gc,2}} = \frac{Q_{gc}}{\Delta T_c} = k_g \frac{w}{2\Delta T_c} \int_0^{d/2\cos\theta} \frac{\Delta T(x)}{\delta(x) + M} dx \quad (21)$$

The local gap thickness can be defined based on the geometry of the contact interface.

$$\delta(x) = \frac{d}{2} - \sqrt{\frac{d^2}{4} - (x\cos\theta)^2} \quad (22)$$

Considering isothermal bounding surfaces , $\Delta T(x) = \Delta T_c$, the thermal resistance, Eq. (21) reduces to:

$$\frac{1}{R_{gc,2}} = k_g \left(\frac{w}{2}\right) \int_0^{d/2\cos\theta} \frac{dx}{\delta(x) + M} \quad (23)$$

The thermal resistance $R_{gc,2}$ can then be calculated by substituting Eqs. (14) and (22) into Eq. (23). This equation can also be used for $R_{g,2}$ by setting $\delta(x) = d/2$ and $\alpha = 2$ (both surfaces are gas):

$$\frac{1}{R_{g,2}} = k_g \left(\frac{w}{2}\right) \frac{((l - (d/\cos\theta))/2)}{(d/2) + \alpha\beta\Lambda} \quad (24)$$

The thermal resistances for the bottom block can be obtained following the same procedure.

$$\frac{1}{R_{gc,1}} = k_g \left(\frac{l\cos\theta}{2}\right) \int_0^{d/2\cos\theta} \frac{dx}{\delta(x) + M} \quad (25)$$

$$\frac{1}{R_{g,1}} = k_g \left(\frac{l\cos\theta}{2}\right) \frac{((w - d)/2\cos\theta)}{(d/2) + \alpha\beta\Lambda} \quad (26)$$

2.3.3. Effective thermal conductivity

Once the individual resistances are determined, the thermal resistance network shown in Fig.5 is used to evaluate the total resistance of the basic cell:

$$R_{tot} = \left[\frac{1}{R_{sp}} + \frac{1}{R_{gc,2}} + \frac{1}{R_{g,2}}\right]^{-1} + \left[\frac{1}{R_{co}} + \frac{1}{R_{gc,1}} + \frac{1}{R_{g,1}}\right]^{-1} \quad (27)$$

The effective thermal conductivity of the GDL is given by:

$$k_{eff} = \frac{d}{R_{tot}A} = \frac{4d}{lwR_{tot}} \quad (28)$$

3. Results and discussion

The model was implemented into a Mathematica script [18] to allow convenient parametric studies and analysis. The thermophysical properties of the gas and carbon fibers used in the program are given in Tables 1 and 2. The gas phase is taken as air to correspond to available experiments used for validation.

Table 1
Properties of air

$\Lambda_{g,\infty}$ (μm)	$k_{g,\infty}$ (W/mK)	T_g (K)	P_g (kPa)	Pr	γ
0.07 [20]	0.03 [4]	350 [21]	101.3 [4]	0.7164	1.398

Table 2
Carbon fiber properties

d (μm)	k_s (W/mK)	ν	E (GPa)	P_{BP} (kPa)
8.5	120 [4]	0.3 [22]	210 [23]	482

3.1. Model validation

Fig. 8 compares the model to experimental data from a variety of sources obtained over a range of porosities. As shown in Fig. 8, there is good agreement between the model and experimental data with an average difference of approximately 7.5% when $\theta = 0$. The model results for three arbitrarily chosen angles are also shown in Fig. 8. The case $\theta = 0$ yields better overall agreement with experimental data and for small fiber angles, the effect of angle is negligible. In an actual GDL, the fiber angle distribution is random and it is expected that the average value would correspond to the orthogonal arrangement, $\theta = 0$, as the present model suggests. This is corroborated by the recent results of Van Doormal [19] who performed Lattice Boltzmann simulation in reconstructed GDLs and observed that the orthogonal arrangement yields permeability values that are indistinguishable from those computed using a random fiber arrangement. The case $\theta = 0$ is therefore selected as the reference case for the parametric studies.

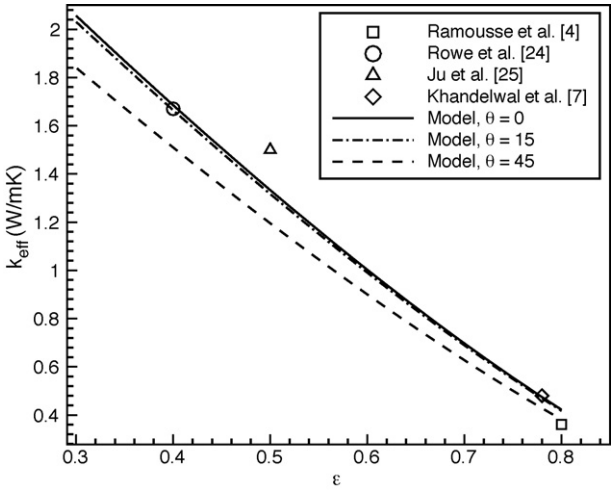

Fig. 8. Comparison of predicted and measured effective conductivities over a range of GDL porosities. (See Refs. [4,7,24,25]).

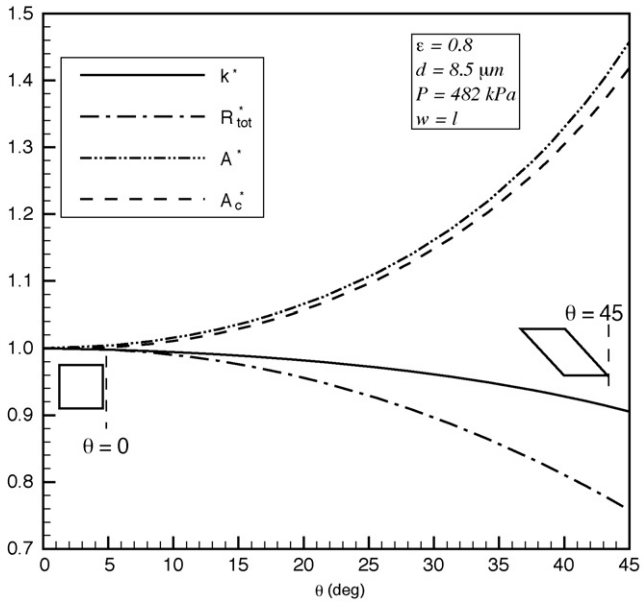

Fig. 9. Effect of fibers angle (θ) on effective thermal conductivity.

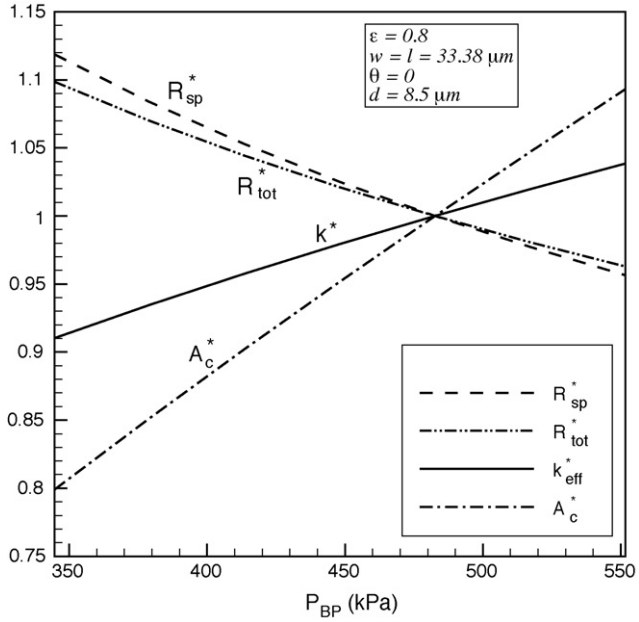

Fig. 10. Effect of bipolar plate pressure on effective thermal conductivity.

3.2. Parametric study

The proposed model can be conveniently used to systematically investigate the influence of key GDL parameters/properties on its effective thermal conductivity. Parametric studies were conducted by varying fibers angle, bipolar pressure, aspect ratio, fiber diameter, and operation temperature. When a parameter is studied, the rest of mentioned parameters are kept constant.

3.2.1. Fibers angle

The preferred conduction path corresponds to smallest resistance which is through the contact between fibers. This path includes spreading resistance; and is hence expected to have a significant influence on the effective thermal conductivity. The effect of fibers angle on the non-dimensional properties of the basic cell is shown in Fig. 9. The properties are non-dimensionalized with respect to the reference case, see Table 3. As shown in Fig. 9, the contact area increases with increasing θ in turn results in a reduction in spreading and consequently, total resistances. However this is counterbalanced by an increase in the basic cell area, and because the latter dominates over the resistance in this case, the net effect is a reduction of the effective thermal conductivity. This effect becomes more pronounced for higher fiber angles.

3.2.2. Bipolar pressure

The effect of bipolar pressure on the thermal conductivity of GDL is shown in Fig. 10. Higher bipolar plate pressures result in higher thermal conductivities. A higher pressure leads to an increase in the contact area that in turn leads to a decrease in the spreading resistance, and thus higher effective thermal conductivity. It should be noted that as a result of increasing pressure, the height of the basic cell is expected to decreases due to elastic compression. However, this effect is small, i.e. a reduction of less than 1% in fiber diameter, thus is neglected in this study. In an operating fuel cell, the compressive force to which the GDL is subjected is expected to vary from a maximum under the land area of the bipolar plate to a minimum under the centre of the flow channel. The sensitivity to pressure shown by the model suggests that the effective conductivity is non-homogeneous and this should be accounted for in comprehensive fuel cell models.

Table 3
The reference case parameters

θ	$w = l$ (μm)	d_0 (μm)	ε	P_{BP} (kPa)	T_g (K)
0	33.38	8.5	0.8	482	350

3.2.3. Aspect ratio

Fig. 11 shows the effect of aspect ratio $\xi = w/l$ for a GDL with a porosity $\varepsilon = 0.8$. As shown, the lower the aspect ratio, the lower the effective thermal conductivity. When the aspect ratio is reduced, in order to maintain the same porosity, l has to be increased while w is decreased, see Eq. (2). This leads to a larger basic cell area, and since the bipolar pressure is kept constant results in larger contact force and hence a lower spreading resistance. Thus the total resistance decreases when the porosity is constant, but this is counteracted by a proportionally larger increase in the basic cell area, and thus a lower effective thermal conductivity.

3.2.4. Fiber diameter

The effect of carbon fiber diameter on the effective thermal conductivity at a constant porosity is shown in Fig. 12. The total resistance decreases with an increase in the fiber diameter. To keep the porosity constant, however, the length and width of the basic cell have to be increased as the diameter increases. Consequently, the area of the basic cell becomes larger and the total thermal resistance decreases. However, a larger diameter leads

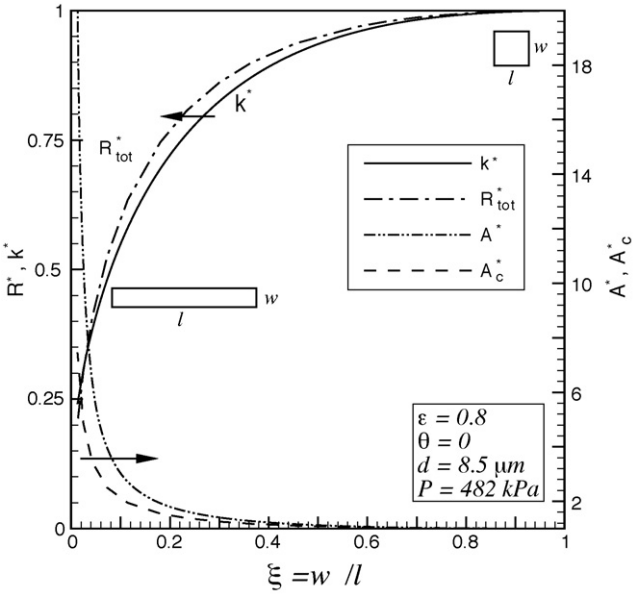

Fig. 11. Effect of aspect ratio on effective thermal conductivity.

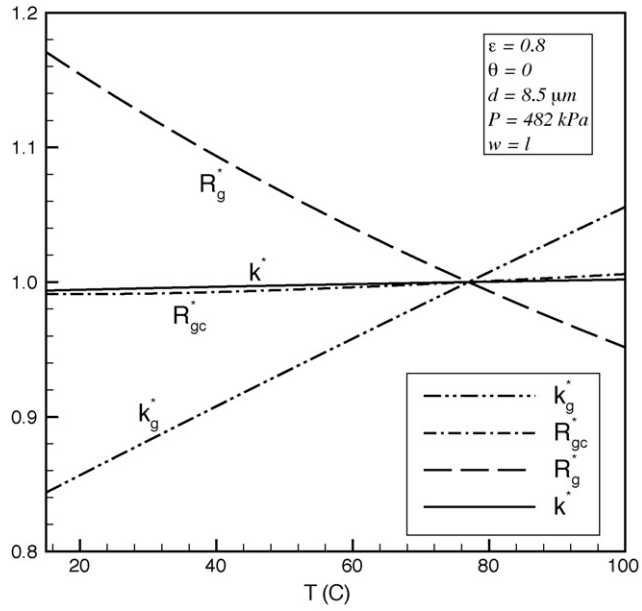

Fig. 13. Effect of the operating temperature on effective thermal conductivity.

to a larger basic cell area which negatively impacts the effective thermal conductivity. Because the effect of the cell height extension and total resistance reduction is higher than the area enlargement, the net effect is a bit increase in the effective thermal conductivity with fiber diameter. In the typical range of 5–10 μm for the fiber diameter, the effective thermal conductivity remains approximately constant.

3.2.5. Operating temperature

Fig. 13 shows the effect of temperature on the effective thermal conductivity. The typical operating temperatures of automotive PEM fuel cell is in the 80–90 ° C range while air cooled and air breathing cells operate at lower temperatures; we thus investigate variations in the 15–100 ° C range. The thermal and mechanical properties of the fiber are assumed to remain constant within this range; however, the effects of temperature variations are considered in gas(air) thermophysical properties e.g. M, k, etc. As shown in Fig. 13, the gap resistance R_{gc} increases slightly with temperature, whereas the gas resistance R_g decreases. The two effects balance each other and also the spreading resistance does not vary, therefore, the effective thermal conductivity remains approximately constant.

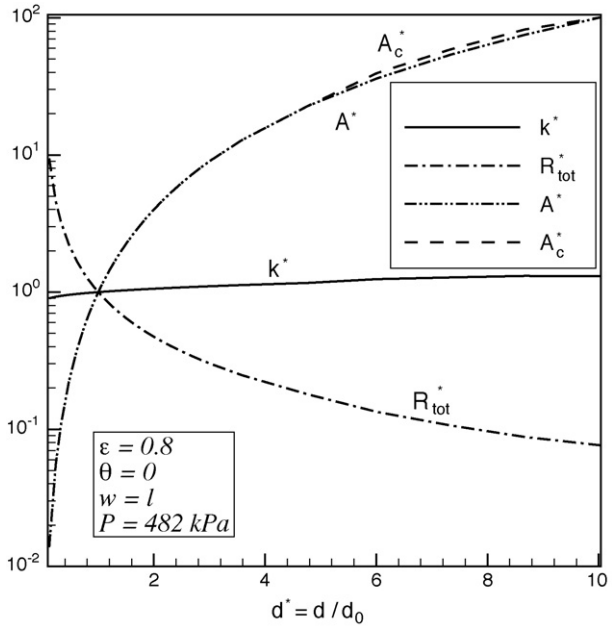

Fig. 12. Effect of fiber diameter on effective thermal conductivity.

4. Summary and conclusions

A compact analytical model for evaluating the effective thermal conductivity of fibrous GDLs has been developed. The model accounts for the salient geometric features, the effect of mechanical compression, and spreading resistance through fibers. The model predictions are in good agreement with existing experimental data over a wide range of porosities, $0.3 < \varepsilon < 0.8$. Parametric studies have been performed using the proposed model to investigate the trends and effects of bipolar plate pressure, aspect ratio, fiber diameter, fiber angle, and operating temperature. The highlights of the analysis are:

- Constriction/spreading resistance is the controlling component of the total resistance.
- Orthogonal arrangement of fibers, $\theta = 0$ yields better overall agreement with experimental data and corroborated by the recent results of Van Doormal [19].
- The influence of fiber angle θ on the effective thermal conductivity decreases at higher porosities.
- Higher bipolar pressure significantly improves the effective thermal conductivity.
- Reducing the aspect ratio, $\xi = w/l$, to approximately 0.7 has a negligible impact on the effective thermal conductivity. However, for $\xi < 0.3$, the effect of aspect ratio becomes important.

The analysis indicates that the best effective thermal conductivity is achieved when $\xi = 1$ (square basic cell).

- Neither changes in fiber diameter (5–10μm) nor operating temperature for the range of 15–100 °C have any significant effect on the effective thermal conductivity.

The compact model presented here, reproduces faithfully the effects of many operational and geometrical parameters on effective thermal conductivity. The model can be used to guide the design of improved GDLs, and can be readily implemented into fuel cell models that require specification of the effective thermal conductivity.

Acknowledgements

The authors are grateful for the financial support of the Natural Sciences and Engineering Research Council (NSERC) of Canada, and the Canada Research Chairs Program. The SEM image in Fig. 1 was provided by Aimy Bazylak.

References

[1] N. Djilali, D. Lu, Int. J. Therm. Sci. 41 (2002) 29–40.
[2] A. Hakenjos, H. Muenter, U. Wittstadt, C. Hebling, J. Power Sources 131 (2004) 213–216.
[3] J.P. Feser, A.K. Prasad, S.G. Advani, J. Power Sources 162 (2006) 1226–1231.
[4] J. Ramousse,S. Didierjean, P. Lottin, D. Maillet, Int. J. Therm. Sci. 47 (2008) 1–8.
[5] B.R. Sivertsen, N. Djilali, J. Power Sources 141 (1) (2005) 65–78.
[6] F. Danes, J.P. Bardon, Revue Générale de Thermique 36 (1997) 302–311.
[7] M. Khandelwal, M.M. Mench, J. Power Sources 161 (2006) 1106–1115.
[8] M. Bahrami, M.M. Yovanovich, J.R. Culham, Int. J. Heat Mass Transfer 49 (2006) 3691–3701.
[9] K.L. Johnson, Contact Mechanics, Cambridge University Press, London, UK, 1985 (Chapter 4).
[10] W. Sun, B.A. Peppley, K. Karan, J. Power Sources 144 (1) (2005) 42–53.
[11] V.S. Arpaci, P.S. Larsen, Convection Heat Transfer, Prentice-Hall, Englewood Cliffs, NJ, 1984 (Chapter 4).
[12] H.S. Carslaw, J.C. Jaeger, Conduction of Heat in Solids, second ed., Oxford University Press, London, UK, 1959.
[13] A.M. Clausing, B.T. Chao, J. Heat Transfer 87 (1965) 243–251.
[14] M.M. Yovanovich, E.E. Marotta, A. Bejian, D. Kraus, in: Heat Transfer Hand Book, John Wiley and Sons Inc, New York, 2003 (Chapter 4).
[15] E.H. Kennard, Kinetic Theory of Gases, McGraw-Hill, New York, 1938 (Chapter 8).
[16] M.M. Yovanovich, Spacecraft Radiative Transfer and Temperature Control, AIAA, New York, 83 (1992) 83–95.
[17] S. Song, M.M. Yovanovich, Fundamentals of Conduction and Recent Developments in Contact Resistance ASME HTD, 69 (1987) 107–115.
[18] Wolfram Mathematica 6, Wolfram Research, Inc., 1988–2007.
[19] M. Van Doormaal, Determination of permeability in fibrous porous media using the lattice Boltzmann method with application to PEM fuel cells, M. Eng. thesis, Queen's University, Kingston, 2006.
[20] M.V. Williams, E. Begg, L. Bonville, H.R. Kunz, J.M. Fenton, J. Electrochem. Soc., A 151 (8) (2004) 1173–1180.
[21] K. Rajashekara, J. IEEE 41 (3) (2005).
[22] H. Miyagawa, C. Sato, T. Masea, E. Drowna, J. Mater. Sci. Eng., A 412 (2005) 88–92.
[23] A. Kusoglu, A.M. Karlsson, M.H. Santare, S. Cleghorn, W.B. Johnson, J. Power Sources 161 (2006) 987–996.
[24] A. Rowe, X. Li, J. Power Sources 102 (2001) 82–96.
[25] H. Ju, C.Y. Wang, S. Cleghorn, U. Beuscherb, J. Electrochem. Soc., A 52 (2005) 1645–1653.